Combustion and Flame 156 (2009) 1480–1492

Contents lists available at ScienceDirect

Combustion and Flame

journal homepage: www.elsevier.com/locate/combustflame

Planar measurements of soot volume fraction and OH in a JP-8 pool fire

Tara L. Henriksen [a,*], Graham J. Nathan [b], Zeyad T. Alwahabi [c], Nader Qamar [c], Terry A. Ring [a], Eric G. Eddings [a]

[a] Department of Chemical Engineering, University of Utah, Salt Lake City, UT 84112, USA
[b] School of Mechanical Engineering, University of Adelaide, SA 5005, Australia
[c] School of Chemical Engineering, University of Adelaide, SA 5005, Australia

ARTICLE INFO

Article history:
Received 10 December 2008
Received in revised form 2 March 2009
Accepted 5 March 2009
Available online 22 April 2009

Keywords:
Incandescence
Fluorescence
Pool fire
JP-8

ABSTRACT

The simultaneous measurement of soot volume fraction by laser induced incandescence (LII) and qualitative imaging of OH by laser induced fluorescence (LIF) was performed in a JP-8 pool fire contained in a 152 mm diameter pan. Line of sight extinction was used to calibrate the LII system in a laminar flame, and to provide an independent method of measuring average soot volume fraction in the turbulent flame. The presence of soot in the turbulent flame was found to be approximately 50% probable, resulting in high levels of optical extinction, which increased slightly through the flame from approximately 30% near the base, to approximately 50% at the tip. This high soot loading pushes both techniques toward their detection limit. Nevertheless, useful accuracy was obtained, with the LII measurement of apparent extinction in the turbulent flame being approximately 21% lower than a direct measurement, consistent with the influence of signal trapping. The axial and radial distributions of soot volume fraction are presented, along with PDFs of volume fraction, and new insight into the behavior of soot sheets in pool fires are sought from the simultaneous measurements of OH and LII.

1. Introduction

This study was undertaken to provide insight into, and new data of, the evolution of soot in buoyancy-driven, soot laden pool fires of JP-8, the kerosene-based fuel used for jet engines. Such information is needed for the development and validation of modern combustion simulations. The spatially resolved measurement of soot volume fraction in turbulent flames from a well-characterized pool fire represents a critical void in currently available validation datasets.

Laser induced incandescence, LII, is reaching maturity as a diagnostic technique in lightly sooting flames [1–4] where it has been used to provide spatially and temporally resolved measurement of soot volume fraction, f_v, in both laminar and turbulent flames [5]. It has recently been extended to determine soot volume fraction in laminar flames at elevated pressures [6–9] and under microgravity conditions [10]. In turbulent conditions, LII has been applied to assess the effects of mixing on soot production using low sooting fuels in both momentum driven and buoyancy dominated flames [11–13]. Shaddix et al. and Shaddix and Smyth used LII to measure soot volume fraction in steady and flickering methane, propane and ethylene diffusion flames [14,15]. Other recent studies have employed LII to determine soot volume fraction in more heavily sooting systems such as in diesel engine exhausts [16–19], and precessing jet bluff body flames of propane [20]. LII has also been employed in a scale model of a gas turbine combustor burning JP-8, by Meyer et al. [21], where the high mixing rates greatly reduce the presence of soot relative to a pool fire.

Murphy and Shaddix [22] provided the first in-situ measurements of soot volume fraction in a large JP-8 pool fire generated from a 2-m pan. These were performed using a semi-intrusive method, with a probe resolution of 5 mm, owing to the challenges of performing LII in such conditions. Xin et al. [23] have recently reported LII measurements in turbulent buoyant flames. However, these data were obtained using methane and ethylene, rather than heavily sooting liquid fuels. Indeed, only limited measurements of soot volume fraction using LII in turbulent jet flames are available [20,24]. There are currently no published LII measurements of spatially resolved soot volume fraction in turbulent flames from pool fires with heavily sooting liquid fuels, such as JP-8.

Schefer et al. [25], Starner et al. [26] and Carter et al. [27] (among others) have shown that the high temperature reaction zone in turbulent jet diffusion flames of hydrocarbon fuels lies in a 0.5 mm thick sheet between the CH layer on the fuel-rich side and the OH layer, on the fuel-lean side. Though more difficult to image, the CH layer is arguably a more precise locator of the reaction zone because it is generally thinner than the OH layer, especially in the tail region of the flame. Carter et al. [27] went to considerable lengths to ensure a soot-free flame for their CH imag-

* Corresponding author. Fax: +1 801 585 9291.
E-mail addresses: thenriksen@exponent.com, vbritelite@hotmail.com (T.L. Henriksen).

0010-2180/$ - see front matter © 2009 Published by Elsevier Inc. on behalf of The Combustion Institute.
doi:10.1016/j.combustflame.2009.03.002

ing. A study by Pickett and Ghandi [11] concluded that the simultaneous imaging of OH and soot could provide a good indication of the location of the high temperature reaction zone. To date, LIF has only been reported qualitatively in turbulent reacting systems, because of the difficulties in correcting for the effects of quenching [5], which would require simultaneous knowledge of the temperature, pressure and collision partners or chemical composition of the flame [28,29]. At the same time, the imaging of OH becomes increasingly challenging with more heavily sooting fuels. This is both because, as a primary oxidizer of soot and its precursors, OH is less prevalent in such flames, and because the interference by scattering from soot particles becomes increasingly strong with more heavily sooting fuels. As a result, to our knowledge no simultaneous soot volume fraction and OH images have been reported in turbulent pool fires of heavily sooting fuels.

To meet model validation needs, the present study aims to provide new, spatially resolved measurement of the distribution of soot volume fraction in a well defined, turbulent pool fire of JP-8. It also aims to provide new insight of the instantaneous spatial relationships between the high temperature reaction zone and soot, using OH as an indicator, in a substantially sooting JP-8 pool fire. Despite limitations of the technique in this application, the results presented here provide a nonintrusive measure of soot volume fraction and OH in situ in heavily sooting pool fires.

2. Experimental

2.1. Burner and fuel

The circular aluminum pool fire pan had a 152 mm internal diameter (ID), 165 mm outer diameter (OD) and height of 76 mm. Cooling water was circulated through the 13 mm shell surrounding the fuel cavity. A batch of 500 L of commercial blend JP-8 was obtained of standard composition. A typical composition for the JP-8 fuel blend is shown in Table 1 [30]. This fuel was fed to the pool fire pan through a 6 mm opening in the bottom of the pan and passed through a fuel dispenser to distribute the incoming fuel with reasonable uniformity. The pan and fuel supply system were securely mounted to a two-dimensional traverse, which allowed the entire system to be traversed through the optical arrangement. A constant fuel level in the pan was maintained by keeping the pool fire pan level with a reservoir can, whose fuel height was maintained by an ultrasonic level sensor. A pump triggered by a PID control program replenished fuel to the reservoir pan. More information on the burner and extinction experiment is reported by Henriksen et al. [34], and on the LII and OH method by Henriksen [31].

2.2. Optical arrangement

The measurements were performed in the diagnostic laboratories of the Fluid Mechanics, Energy, and Combustion Group at the University of Adelaide. The fundamental output of a Nd: YAG laser provided an infrared (IR) beam at 1064 nm with a pulse width of 5 ns. A series of cylindrical and spherical lenses were used to expand the incoming IR beam into a 0.5 mm weakly diverging sheet in one plane that measured 85 mm tall by 1 mm wide in the image plane, which passed through the center of the flame. The size of this sheet was chosen to ensure that the intensity throughout this region was within the plateau region of the fluence curve (described below), whilst providing larger sheets than the 45 mm possible with a parallel sheet for the simultaneous images with OH. The LII images were recorded with an ICCD camera (ICCD-576-G/1, Princeton Instruments) operated at a 40 ns gate width and zero gate delay. The gate of the camera was triggered by the Q-switch of the ND: YAG laser to ensure that the laser pulse arrives at the start of the gate. A zero gate delay was chosen to avoid bias towards larger particles caused by long or delayed detection. An interference filter with a center wavelength of 430 nm and a 10 nm bandwidth (Andover) was used to suppress any C2 LIF during signal detection.

The recorded image was clipped at the data processing stage, to minimize power losses due to edge effects. After the clipping procedure, the volume imaged by each pixel was $0.625 \times 0.625 \times 1$ mm, resulting in an imaged area of 50 mm $\times$ 360 mm. The relative signal to noise ratio (S/N) was 50. Approximately 1000 pictures were taken by the ICCD camera for each height in the turbulent flame.

The second harmonic output radiation (532 nm) of a pulsed Nd: YAG laser (Brilliant B, Quantel) was used to pump a tunable dye laser (Lambda Physik SCANMATE, utilizing Rhodamine 6G dye) near 565 nm, producing short ($\sim$5 ns), narrow bandwidth ($\sim$0.08 cm^{-1}) pulses. The output beam passed through a BBO (frequency doubling) crystal and the fundamental fraction was separated by a Pellen Brocca prism and discarded. The frequency doubled laser radiation, at 281.4 nm [29], was directed through a cylindrical telescope lens system to produce a sheet of $\sim$0.5 mm thickness and sufficient uniformity, and passed through the center of the flame. The (1–1 and 0–0) fluorescence, near 307 nm, was collected by a UV lens, after transmission through a band pass filter (bandwidth 10 nm FWHM) and a dichroic filter. This combination was found be very effective at minimizing interference from PAH excited molecules. The transmitted fluorescence was imaged onto a gated intensified CCD camera (Princeton Instruments ICCD-576) orthogonal to the laser sheet. A gate width of 50 ns was used, well below the 100 ns required to reduce background flame radiation relative to the noise floor.

Online (the precise spectral wavelength required to excite OH) and offline measurements were recorded at various heights in the flame to determine a signal to noise ratio of 3. For simultaneous imaging, the LII camera was adjusted to offer an imaged area (99 $\times$ 246 mm) more closely corresponding to that provided by the LIF camera (88 $\times$ 133 mm). The resolution limitations of the LIF camera resulted in only a portion of simultaneously overlapped spatial region in the flame. This simultaneously imaged position spanned from the center of the flame to $r/d \approx 0.8$, where d is the pan diameter and r the radius.

The laser fluence was measured for the LII sheet passing through a laminar ethylene co-flow flame. The intensity (Fig. 1) was measured on the LII camera as the power of the laser was slowly increased by use of neutral density filters. The plateau region occurred between 0.4 J/cm^2 (thin black arrow) and 1.1 J/cm^2. Instantaneous LII images were collected while operating at 1.3 J/cm^2 near the end of the fluence curve, and simultaneous measurements operated with an LII excitation power source of 1.01 J/cm^2, with position indicated by the thick arrow in Fig. 1. The standard deviation of the plateau region was 5.8%, and the maximum uncertainty due to laser power fluctuation on the LII signal was determined to be 14%, which is much less than the calibration error (22%) associated with the technique (Section 2.3). As such, no laser

Table 1
Composition of JP-8 jet fuel.

	Wt%
n-Paraffin	~28
Branched paraffin	~29
Mono-aromatics	~18
Diaromatics	~2
Cycloparaffin	~20
Nondetermined	~3
Total	100

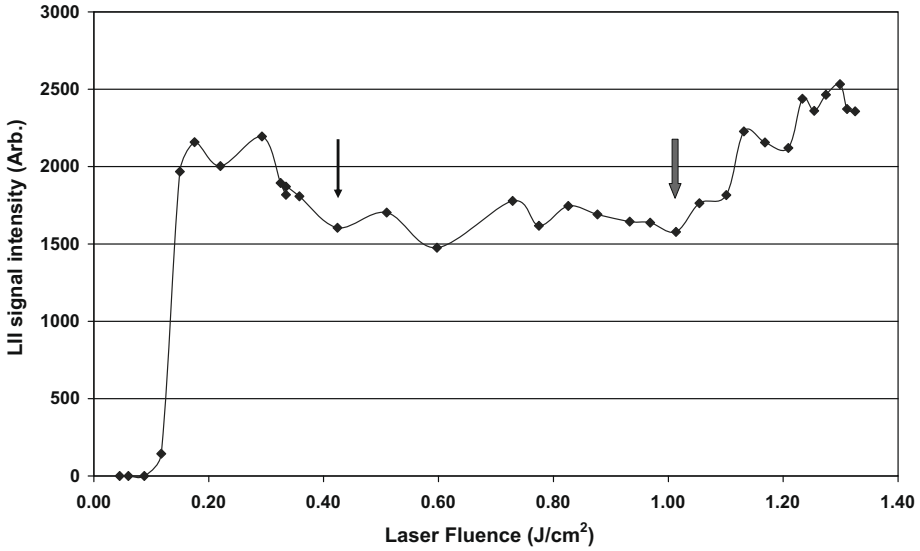

Fig. 1. Laser fluence (J/cm^2) obtained from an ethylene co-flow burner for the optical system used in the LII and LII/LIF experiments. The thick arrow indicates the operation intensity of the laser during simultaneous imaging. The thin arrow represents the beginning of the plateau region.

power corrections were required to quantify the soot volume fraction from LII.

2.3. Calibration and uncertainty

A line of sight extinction experiment was used to calibrate the relative LII signal to absolute soot volume fraction in a laminar JP-8 diffusion flame using the method described by Choi and Jensen [32]. A stainless steel tube with a 25 mm OD formed the base of a burner with a height of 38 mm. This pan was mounted atop a co-flow burner to utilize a nitrogen shroud as is required to keep the flame steady. The co-flow burner was securely mounted to a two-dimensional traverse. The pan was filled to the top with liquid fuel and then lit and allowed to burn transiently for 5 min until the flame stabilized. The heat loss to the burner during the experiments was not measured but was judged to have approached a steady state prior to the start of all laser experiments. A pseudo steady state was approximated when the flame appeared to be steadily burning with a well-defined boundary. It should be noted that, due to the use of a fixed volume of a blended fuel, true steady state is not possible, since the lighter fractions will vaporize first.

The extinction measurement was performed using a continuous wave 532 nm laser diode, operating at 10 mW with a beam diameter of 5 mm (unfocused) that passed through a series of three 50/50 beam splitters. The beams were oriented at angles of 0°, 45°, and 90° to each other, and aligned to cross on the axis of the flame. A fourth beam provided a reference to correct for possible variations in the temporal laser power intensity. Filters and apertures were placed in front of each of the four photo-detectors to minimize radiative interference from the flame. The ratio of the average value of the incident to attenuated beams yields the average attenuation, which is related to the average soot volume fraction in that part of the flame. The line of sight soot volume fraction, $\bar{f}_v$, was determined according to the following equation:

$$\frac{I}{I_0} = \exp\left(-K_e \frac{\bar{f}_v}{\lambda} L\right) \tag{1}$$

where I and I_0 are the attenuated and reference signals respectively, L is the optical path length, and λ is the wavelength of light. The scattering contribution (extinction coefficient) for the soot particles (K_e) was assigned the value of 9.87 for JP-8 soot, as measured by Zhu et al. [33]. Extinction in the laminar flame was measured at two axial locations, 5 and 19 mm. The laminar burner was extinguished between each set of axial measurements to replenish fuel. A more detailed presentation and discussion of the laminar extinction results and optical path length is reported by Henriksen et al. [34]. The time averaged extinction levels through the laminar JP-8 flame were measured to be approximately 9–11%. These results were found to be acceptable levels of extinction to justify the use of the laminar flame for calibration. Time averaged and peak instantaneous extinction measured in the JP-8 pool fire, in contrast, was measured to be 35–50% and 70%, respectively, requiring the use of the Choi and Jensen [32] method to obtain a reliable calibration.

The calibration constant (C) determined from the laminar flame provided a means to quantify soot volume fraction from the LII technique in the pool fire. The effects of signal trapping and fluence variations through the plateau region were estimated to contribute ~14% to uncertainty in the LII measurement, as calculated from the maximum uncertainty of the fluence curve. However, the uncertainty in the calibration constant bounds the error on the measurement at 22%. The calibration constant was calculated by averaging the calibration constants determined at two heights in the JP-8 laminar flame. The percent error on the calibration constant was estimated by projecting the extinction variance through the determination of the calibration constant. This average calibration constant was determined to be $1.18 \times 10^{-9} \pm 2.6 \times 10^{-10}$ a.u.

An assessment of the overall experimental uncertainty of the LII measurement was obtained by comparing the extinction through the flame derived by LII with those measured directly by the extinction experiment. It can be seen from Fig. 2 that the LII derived measurement is consistently lower than the direct measurement, with an average difference of 21%. This difference may be caused by PAH absorption, which is known to be more significant in the visible than the IR. Signal trapping, which acts to attenuate the signal between the laser sheet and the camera in the LII measurement, may also play a role. However, since the average overall difference between the two methods was less than the calibration constant error quantifying soot volume fraction, the application of a correction factor would not improve accuracy, and was therefore not appropriate.

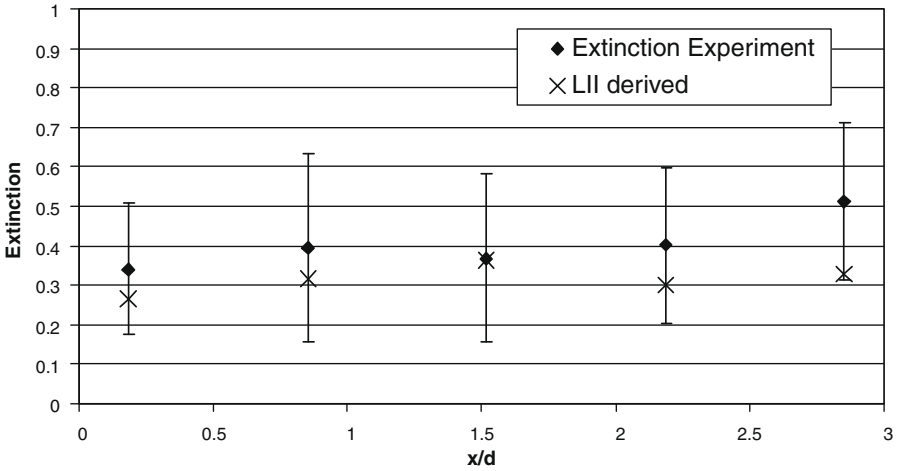

Fig. 2. A comparison of the direct extinction measurement with that derived from the LII measurement for the JP-8 pool fire.

3. Results and discussion

3.1. Calibration results

Measurements of soot volume fraction averaged across the entire path of the flame were performed by an extinction experiment without applying an Abel transform based on radial measurements through the flame [32]. Such a measurement only equates to local soot volume fraction values when the soot is uniformly distributed along that path, a condition not satisfied by the JP-8 laminar flame.

The path length used to calculate the JP-8 soot volume fraction in the laminar flame was measured from the LII images, which can be used to precisely define the dimensions of the two separate soot sheets that attenuated the laser beam in the extinction experiment. The soot volume fraction is then determined from the calibration constant (which relates the intensity of soot in the LII image to the attenuation measured from extinction) and the LII pixel intensity, according to the following equation:

$$f'_v = C * I \tag{2}$$

The instantaneous peak soot volume fraction, $f'_{v,\max}$ of 2.57 ppm occurs at an axial position $x/d = 1.40$ for the JP-8 laminar flame. A time averaged image offers a relative means of identifying regions in the flames corresponding to consistently higher amounts of soot volume fraction. The time averaged soot volume fraction is shown for the JP-8 laminar flame in Fig. 3, where the $\bar{f}_{v,\max}$ of 1.75 ppm occurs at an axial distance $x/d = 1.01$. The JP-8 laminar flame has a diffused cone like shape, where the bulk of the soot is concentrated in the center, just above the vapor dome. The higher value of $f'_{v,\max}$ as compared to $\bar{f}_{v,\max}$ is consistent with the expectation of varying local soot concentration in a transient system. However, the instantaneous soot volume fraction is an order of magnitude higher than that report by Shaddix and Smyth (0.33 ppm) for a laminar methane diffusion flame [15]. This is somewhat expected, since JP-8 is a substantially more sooting fuel than methane.

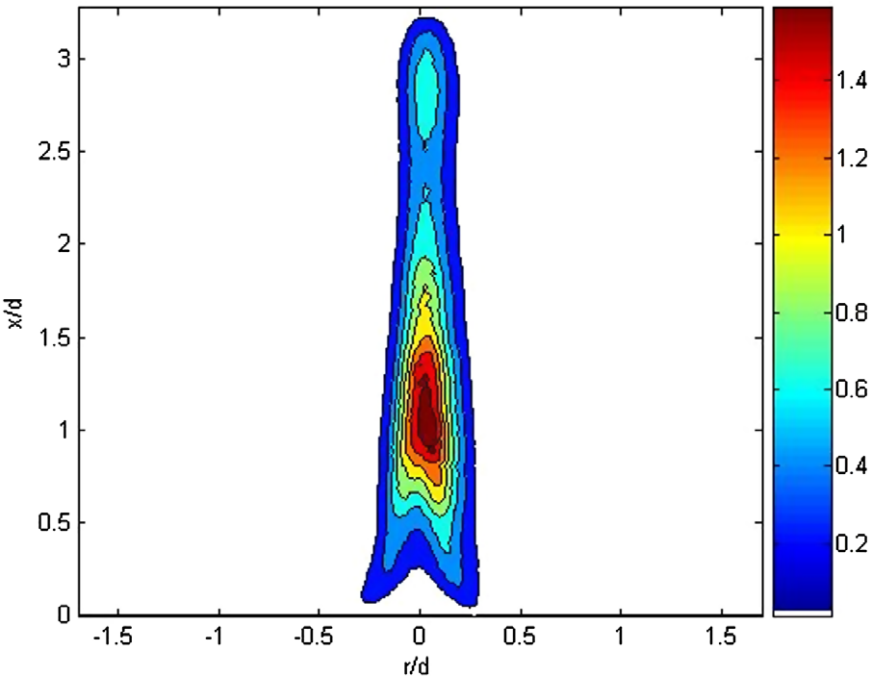

Fig. 3. Collage of time averaged soot volume fraction (ppm) from laminar JP-8 diffusion flame averaged from 250 images (over 5 min).

3.2. LII results

A collage of the time averaged soot volume fraction in the pool fire (each averaged over 1000 images) is shown in Fig. 4. The soot volume fraction was determined by multiplying the LII intensity by the calibration constant. The peak value of time averaged soot volume fraction, $\bar{f}_v$, in the JP-8 pool fire was measured to be 0.40 ppm, and this value occurred close to the burner at $x/d = 0.004$. This value is comparable to the $\bar{f}_v$ value (0.77 ppm) calculated from an emission measurement by Murphy and Shaddix [22], 0.1 m from

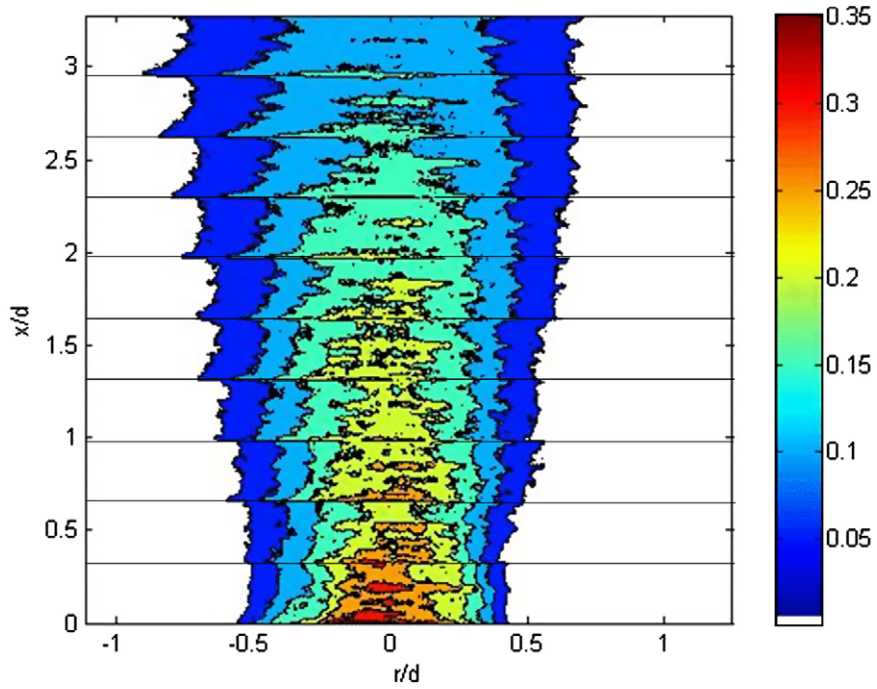

Fig. 4. Collage of time averaged soot volume fraction (ppm) from turbulent JP-8 pool fire from 1000 images (over 20 min) at 10 heights.

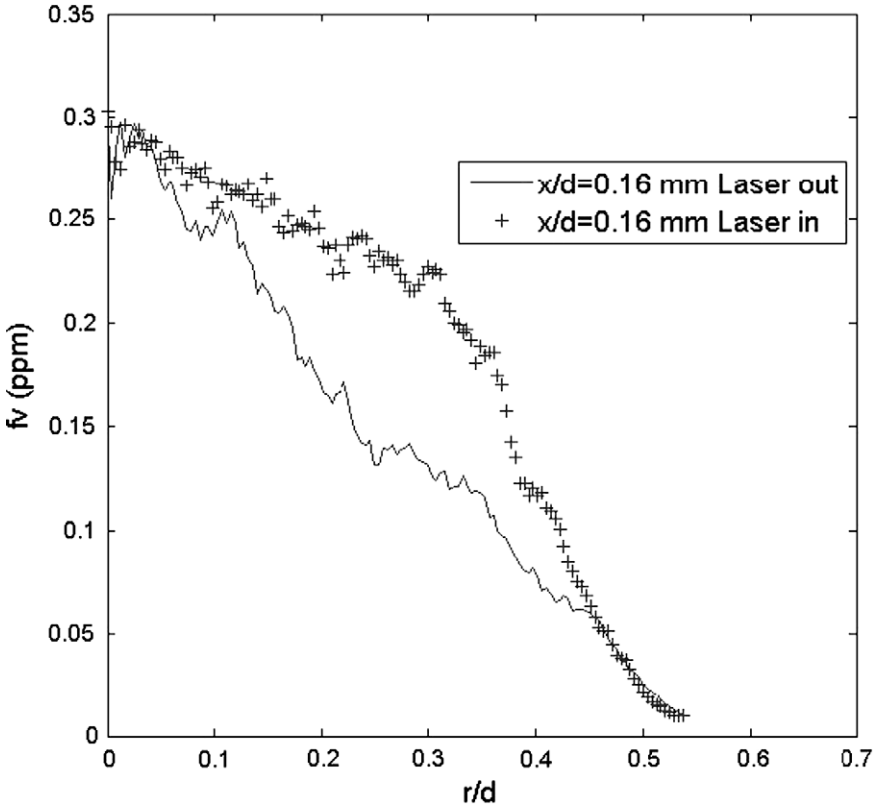

Fig. 5. Time averaged radial distribution of soot volume fraction (ppm) in a JP-8 pool fire, at height 1, approximately 25 mm from the base of the pan.

the centerline in a 2 m JP-8 pool fire using a semi-intrusive probe. Also for comparison, Qamar et al. [28] reported LII measurements of peak time averaged soot volume fraction in a 6 mm turbulent natural gas flame (DEFLT) of 0.15 ppb. The magnitude of the difference in f_v between these two burner types is not surprising, as results from this study and others by Qamar et al. [20] demonstrated that high strain rates result in generally lower local soot volume fraction. The axial and radial distribution of f_v viewed in the collage reveals that more soot is found near the base of the pan and in the center of the flame. The imperfect matching of the time averaged collage images at the edges of successive sheets is attributed to variations in laser fluence through the sheet, due partly to laser sheet broadening (7%), and to extinction losses through the flame. These effects contribute to a "saw toothed" shape in the time averaged profile, which is slightly more pronounced on the left side (laser-out side) of Fig. 4. These effects were reduced, but not eliminated, by clipping the images from 85 to 50 mm in height for the data extracted from the images.

To assess the relative symmetry of the soot distributions as measured on the laser-in and laser-out side of the flame, and to assess power losses through the flame, radial plots were analyzed at each of 10 heights [31], though only data for one height is shown in

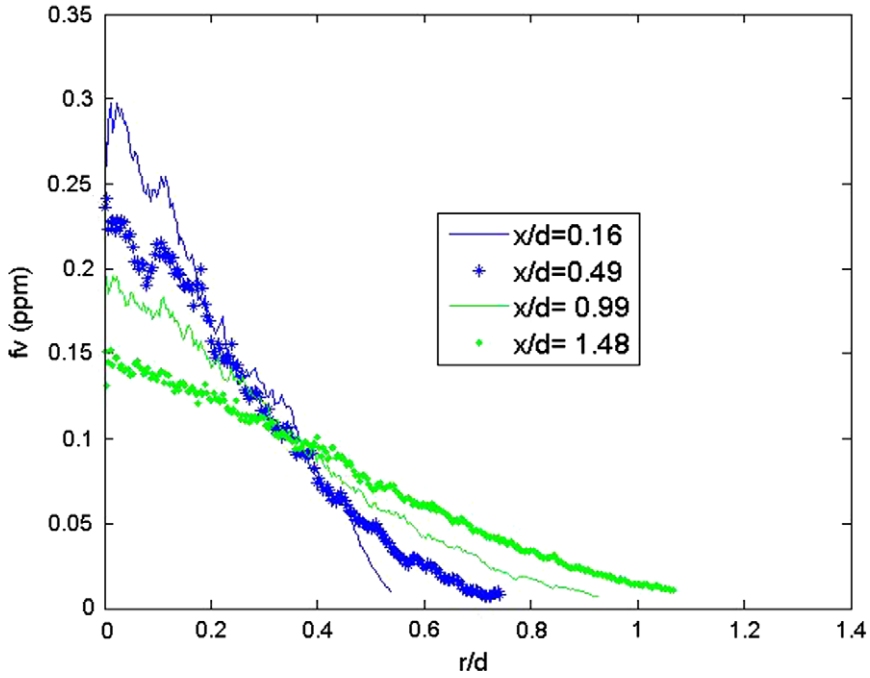

Fig. 6. Axial distribution of time averaged soot volume fraction radially integrated from the edge of the flame to the centerline of the JP-8 pool fire. Each point on the line represents a planar integral at a fixed height.

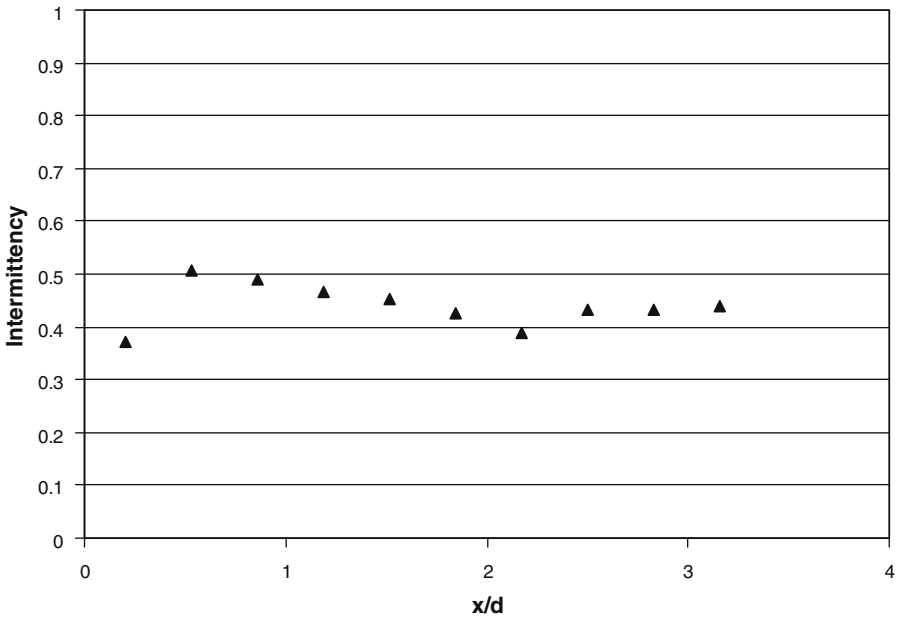

Fig. 7. Intermittency as a function of height along the centerline of the JP-8 burner axis.

Fig. 5. Consistent with the time averaged collages, the radial distribution of $\bar{f}_v$ exhibits a peak at the center (as depicted in [31]), and decreases toward the edge of the pan. The symbols in Fig. 5 denote the measurements on the laser-in side of the axis, while the solid lines denote the values on the laser-out side. The intensity of the laser-in side is slightly greater than the laser-out side due to losses of the light signal attributed to attenuation, so the laser-in values are considered to be the more reliable of the two.

Following Qamar et al. [20], Fig. 6 presents the axial distribution of total time averaged soot per mm of flame height. It represents a double integral of $\bar{f}_v$ through concentric rings at each unit height from the edge of the flame to the centerline. That is, each point in Fig. 6 represents the total soot in a plane parallel to the fuel surface and the integral under the curve represents the total soot volume in the flame. The integrations were performed only from the laser-in side of the data, assuming that the soot is axisymmetric in the mean, which is a reasonable assumption. It is evident that the total amount of soot in the JP-8 flame exhibits a slight decrease in the first half-pan diameter, and then increases with height by about 40% to remain approximately constant near the flame tip. This trend is quite unlike the measurement in jet flames [20], in that the soot here does not exhibit any net burnout in the region of the flame tip. However, it is consistent with the broadening of the JP-8 soot profiles with increased height (Fig. 4) and with the visual observation of the increased presence of soot outside the flame envelope with increasing height, including above the flame tip. It is also consistent with previous measurements of total extinction in this flame [31,34].

To further assess the distribution of soot in the turbulent flames, the axial distribution of intermittency, I_n, along the centerline is presented in Fig. 7. Here I_n is defined as the probability of not finding soot at a given location. It was calculated by binarizing the LII measurements. A value of 0 was assigned to values above an intensity threshold, corresponding to the presence of soot, while a value of 1 was assigned to any intensity values below this threshold, corresponding to the presence of no soot. The threshold (100 counts on the ICCD array) was chosen by systematically interpolating its value until no effect on intermittency trends was observed. It is evident that the intermittency of soot in the JP-8 pool fire is nearly constant with height. Its value $0.4 < I_n < 0.5$, represents a high probability of finding soot everywhere. This is much higher than the values $I_n > 0.97$ reported by Qamar et al. [28] for a methane jet flame, consistent with a much higher soot loading in the JP-8 flame.

The probability distribution of the local instantaneous soot volume fraction was also measured along the centerline at 10 different axial locations in the flame. The probabilities were calculated by binning a sample of 4×5 pixels along the centerline to provide reasonably converged statistics. The log of the probabilities of soot volume fraction is presented in Fig. 8. The symbols represent data, while the lines represent the lines of best fit based on an exponential function. It is evident that in each case, the data is reasonably well described by an exponential function (not unlike those used in population modeling) with typically a 95% fit to the data, which was clipped at values of zero for illustrative purposes. In some cases there is a slight departure from the exponential function at low f_v, with a slight peak evident at $f_v > 0$. This is in contrast to the flames with much lower soot loadings reported by Qamar et al. [24,28], in which all pdf's followed an exponential distribution. However it is to be expected that flames with low values of I_n will not have a most probable value of $f_v = 0$.

It is evident from Fig. 8 that the maximum instantaneous values of soot volume fraction, $f'_{v,\max}$ is approximately 2.5 ppm. This is an order of magnitude higher than the averaged maximum value ($\bar{f}_{v,\max}$) of 0.4 ppm, but is still slightly lower than was mea-

Table 2
Coefficients for determining the best-fit equation for the JP-8 probability function.

x/d	A	B
0.205052	0.0875	−0.0024
0.533136	0.0875	−0.0024
0.86122	0.0866	−0.0028
1.189304	0.0759	−0.0026
1.517388	0.1242	−0.0036
1.845472	0.1496	−0.0041
2.173556	0.1714	−0.0048
2.50164	0.1687	−0.0053
2.829724	0.3264	−0.0079
3.157808	0.2018	−0.0071
Avg.	0.1480	−0.0043

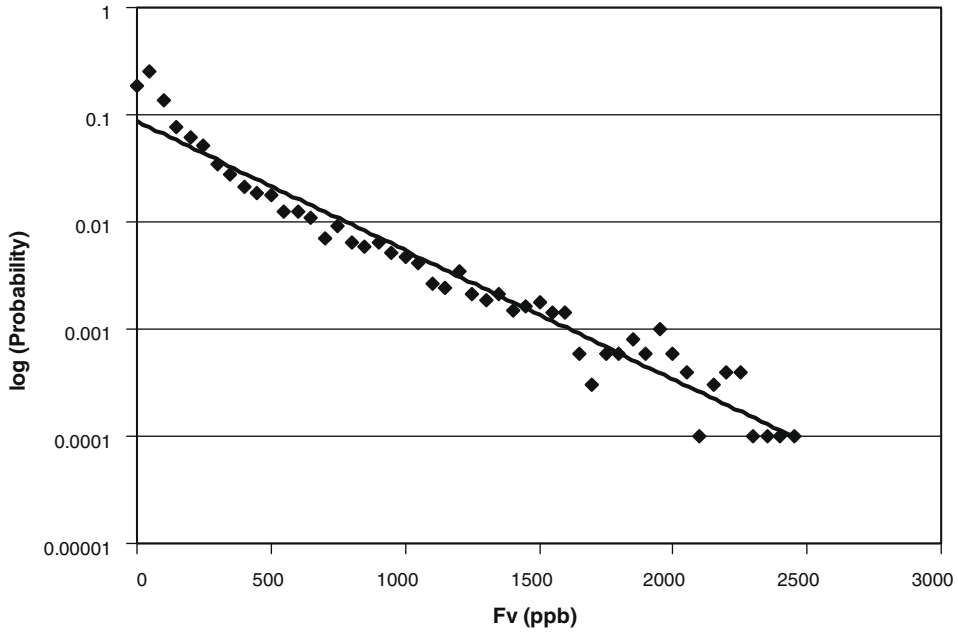

Fig. 8. Log of the probability of soot volume fraction in a JP-8 pool fire at a height 1 ($x/d = 0.20$).

sured for the laminar flame (2.6 ppm). It is comparable with the peak values of 2 ppm measured for a methane flickering flame, and significantly lower than the 8.5 and 18 ppm measured for propane and ethylene flickering laminar flames [14,15]. Given that the values of $f'_{v,\max}$ measured for turbulent flames of propane were around 4 ppm [20], and that JP-8 is a heavily sooting fuel, the present measurement seems to be somewhat low. This difference may be, in part, due to the effects of signal trapping, as discussed above.

The exponential best-fit function for the PDF of soot volume fraction in Fig. 8 is given by Eq. (3), where P_b is the probability and f_v is the soot volume fraction. The constants A and B are dependent on the height of the measurement, and are defined in Table 2.

$$P_b = Ae^{B*f_v} \tag{3}$$

A complementary view of the variation in the soot volume fraction with axial distance can be seen in the three-dimensional plots of Fig. 9, shown on a three-dimensional scale. The probability of finding no soot along the centerline varies from between 0.17 and 0.25 and exhibits essentially the same profile as the intermittency for JP-8 shown in Fig. 7, but with slightly lower values, corresponding to a different threshold. The non-zero peak in the probability of f_v occurs near the base of the burner where $\bar{f}_v$ is greatest and where I is lowest. That is, for this flame, the most probable value of f_v is zero for situations where the soot loading is not too great, here corresponding to $I \geqslant 0.45$, but greater than zero for lower values

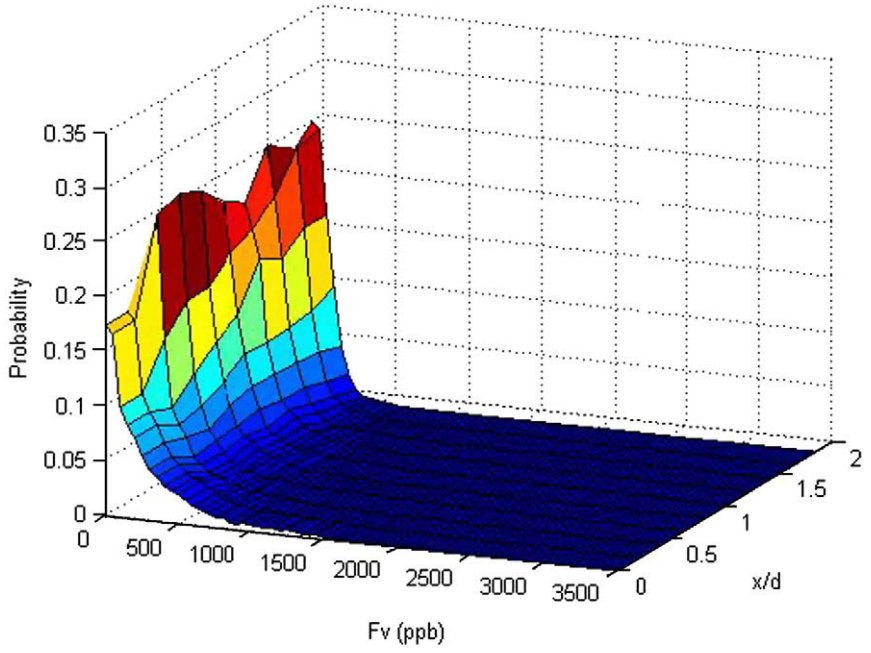

Fig. 9. Probability of soot volume fraction (ppb) along the centerline at varying axial locations in the JP-8 turbulent flame.

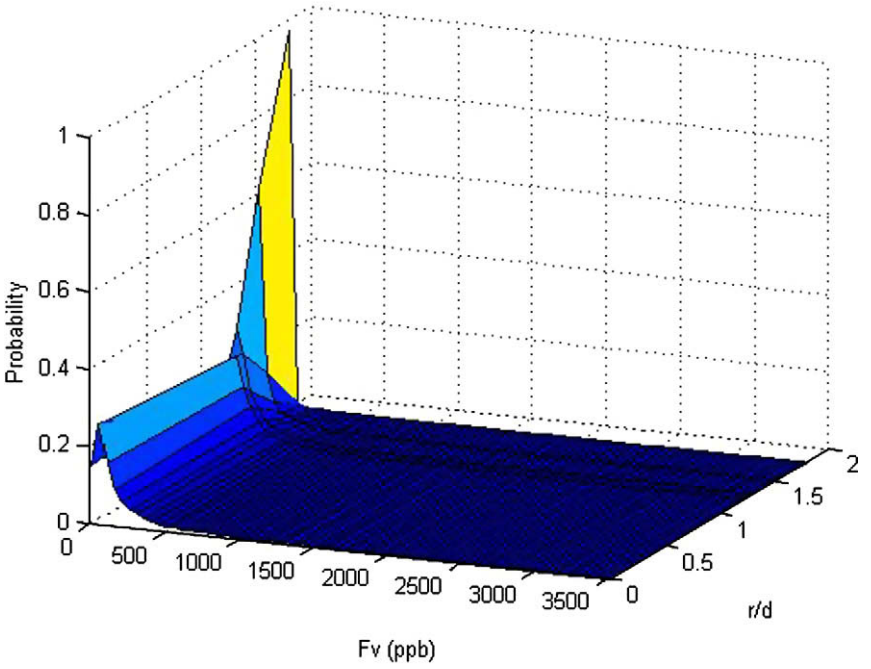

Fig. 10. Radial distribution of the local soot volume fraction from the centerline to the flame's edge at $x/d = 1.2$ in the JP-8 flame.

of I. The probability of finding higher values of f_v tends toward an exponential decrease from the most probable value of f_v, although it departs somewhat from the exponential function close to the peak value.

The radial trends of local soot volume fraction probability distribution are shown in Fig. 10, also on a linear scale, at the first measurement height. The shape of the distribution is approximately constant for $r/d < 1$, i.e. until the edge of the flame is approached. Toward the edge, the intermittency increases dramatically, reflecting fluctuations in the outer envelope, and a rapid increase in the probability of finding no soot there. Commensurate with this increase, the slope in the decay function changes dramatically.

3.3. Simultaneous imaging results

For the simultaneous images, the LIF camera was aligned to image an area of 88 mm × 133 mm, corresponding to just over half the flame width on the laser-in side. As for the LII alone, one thousand image pairs were collected at each of eight heights. The LII images were calibrated, while the OH is reported in arbitrary units (a.u.), as described above. The LII and LIF images were overlapped using a common grid, imaged cold. A typical example of an image pair at the base of the flame is shown in Fig. 11, with the two images separate, and in Fig. 12 with the images spatially overlapped. For clarity OH is shown in gray scale while the LII is shown in color. It is evident that the OH sheet is found radially on the outside of the

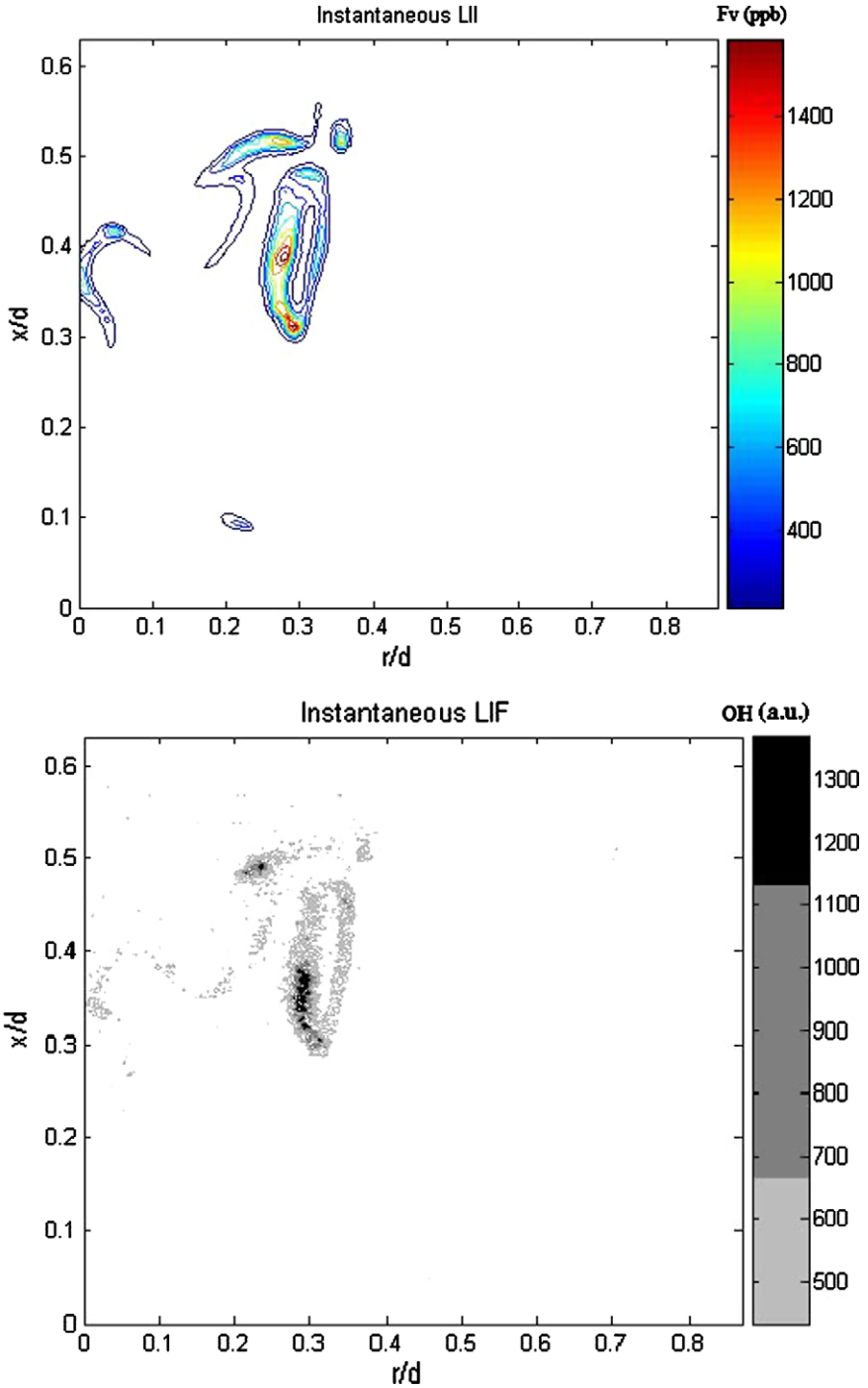

Fig. 11. A typical example of an instantaneous and simultaneous image of LII (top) and OH LIF (bottom), recorded at the base of the flame.

soot sheets, with good matching of their shapes. This is consistent with the general expectation for this region of the flame where little unburned soot is found outside the visible flame envelope, where OH marks the oxidizer side of the reaction zone and the soot marks the fuel-rich side. It is also evident that despite the relatively poor signal to noise ratio, the OH can be discriminated from the soot because of the spatial separation of the two species.

By visual inspection of the entire set of simultaneous image pairs, four categories of the spatial relationship between the soot and OH sheets were identified. These are:

I. OH is only present on the outside (right hand side) of the soot sheet
II. OH is present to the right and left/top/bottom of the soot sheet
III. Soot appears to be "breaking through" an OH region
IV. There is a strong visual correlation in the shape of the soot and OH sheets.

Examples of each category are shown in Figs. 13–16. Of these classifications, only the first and last are mutually exclusive. A sample of approximately 130 simultaneous images from various heights was assessed statistically, and the results are shown in Fig. 17. Though subjective, some consistent and interesting trends are apparent. Firstly, the shape of the OH distribution is strongly correlated with that of the soot sheets in general, although this de-

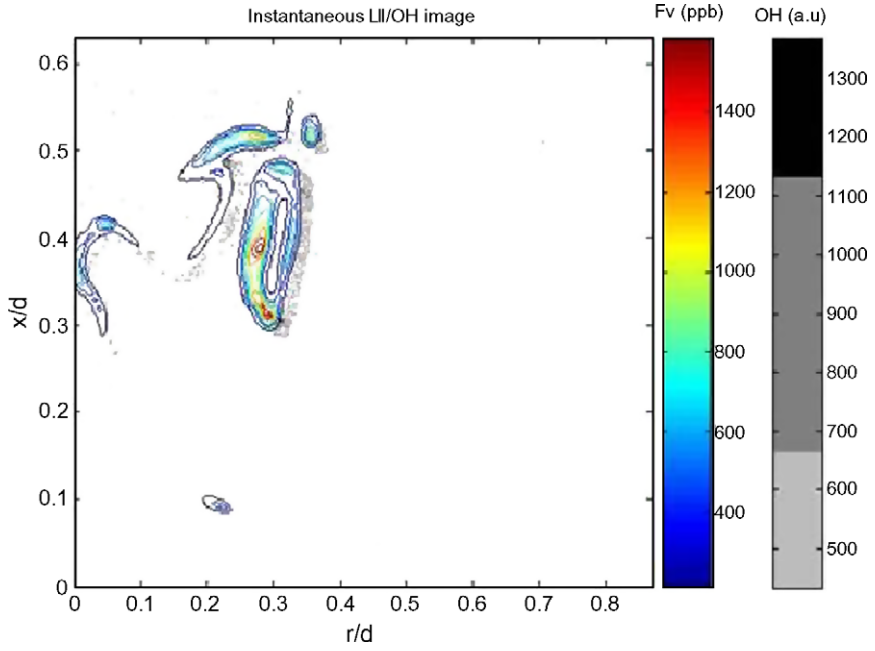

Fig. 12. Overlapped images from figure.

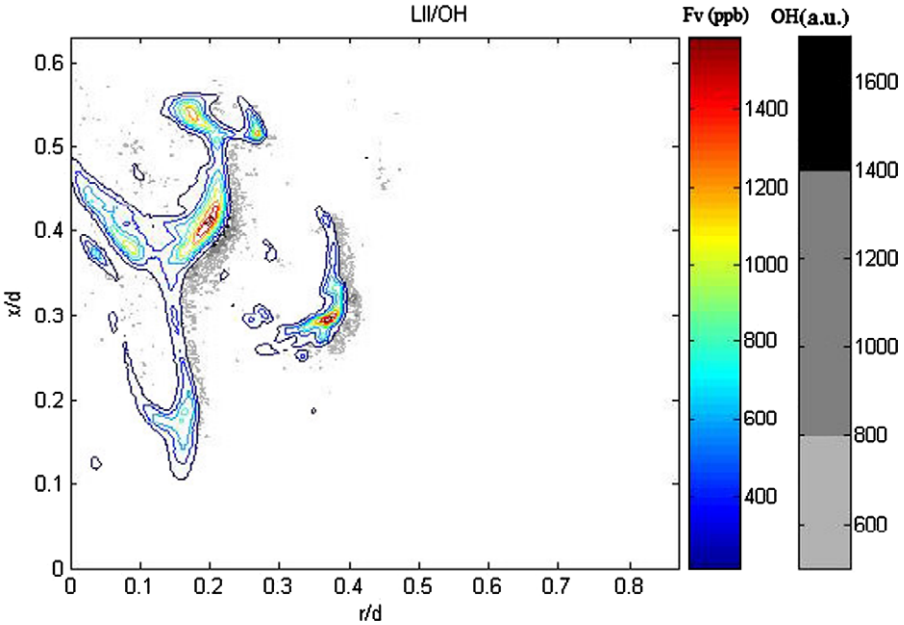

Fig. 13. Example of category I, OH on the right side of soot.

creases from 80% at the flame base to 60% at the flame tip. There is also a definite trend that the probability of OH being only located radially outside (on the RHS) of the soot sheets, decreases with increased height from around 60% near the base, to approach zero near to the tip. Commensurate with this, the probability that soot is found to the right and above, below, or to the left of the sheet is found to increase with height. This is consistent with increased dynamics of the flame with height. Overall 30% of the images show OH only to the right of soot sheets, with 48% of the images revealing OH to the right and at another position (top, bottom or left). The sum of these categories is also presented in Fig. 17. The difference between this and 100% corresponds to the percentage of time for which soot is found without OH on the outside of it. This, presumably, corresponds to unburned soot that has escaped from the flame envelope. With increased axial height above the burner, an increasing number of images revealed broad distributions of OH, rather than sheets. Broad regions of OH may correspond to disassociated water in hot combustion products. In 21% of the images that were analyzed, soot could be seen apparently "breaking through" the OH sheet. However, none of these events were found to occur in the base of the flame. Rather they tend to be increasingly probable with height, to become about 35% probable at the tip. Overall, these observations reveal a consistent trend of the important – if not dominant – role of the large-scale dynamics of the flame, which become increasingly strong with height under the action of buoyancy, in the escape of unburned soot from the flame.

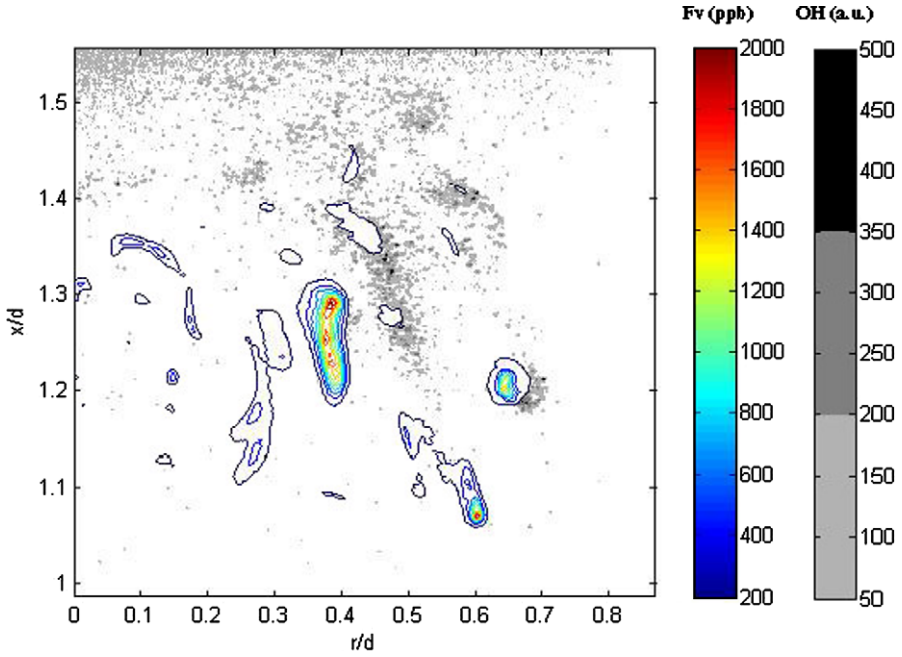

Fig. 14. Example of category II, OH on the right, top and bottom of soot.

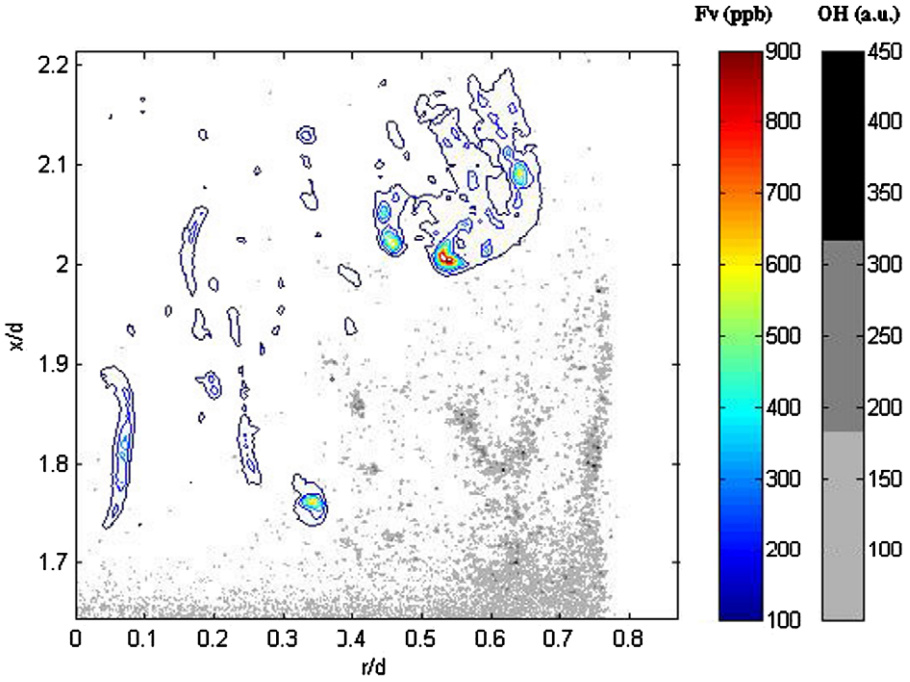

Fig. 15. Example of category III, soot sheet breaking through OH.

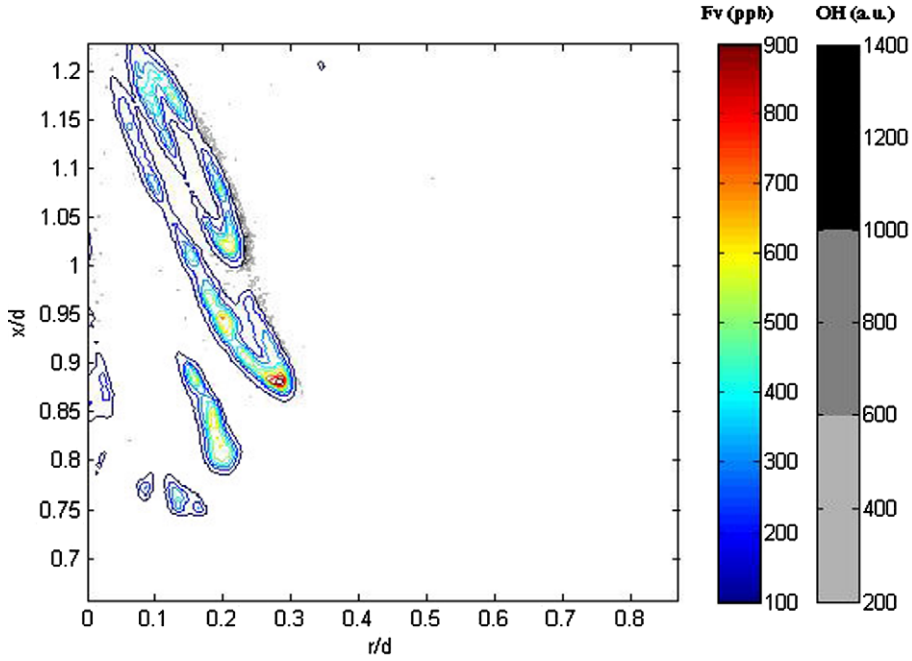

Fig. 16. Example of category IV, a strong visual correlation between OH and soot.

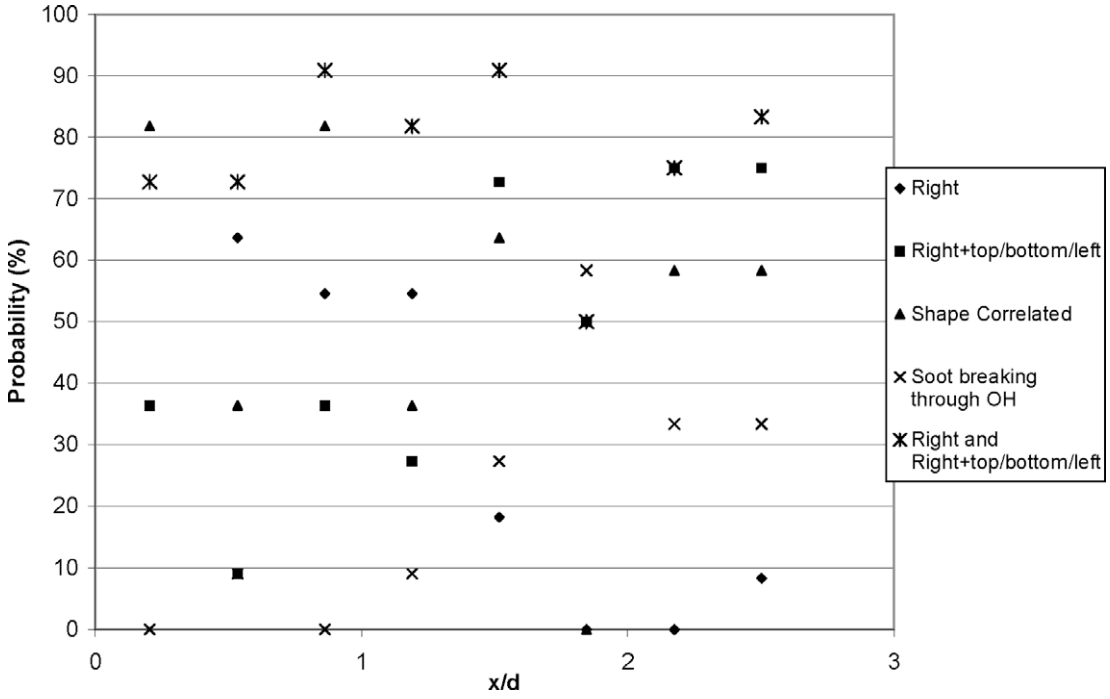

Fig. 17. Trends of OH position relative to soot sheets and trends of soot breakthrough with height in the JP-8 flame.

The distribution of soot in Fig. 12 bears some resemblance to that in the 2-D shear layer investigated by Pickett and Ghandhi [11]. In their Fig. 2, the soot distributed in large blobs was found to be associated with the "cores" of the coherent, vortical structures in the shear layer, which are connected by thinner "braid" regions. The size of the apparent core in Fig. 12 is too small to be a primary puffing motion, so it may be linked to a smaller "seeding vortex". Pickett and Ghandhi [11] also found that particular flow conditions and large-scale flow features were associated with the strong correlation between the shape of the OH and soot sheets. While the conditions in the shear layer are too different from those in the pool fire to allow a direct comparison, this is further evidence of the importance of large-scale flow dynamics.

4. Conclusions

Measurements of soot volume fraction were performed in a heavily sooting pool fire of JP-8 with total average extinction of

35–50% and peak instantaneous extinction of up to 70%. It is not yet realistic to correct for the effects of signal trapping in a turbulent flame, which, under these conditions, are significant. Calibration was performed against a small laminar pool fire of JP-8 using Choi's method [32] to account for signal trapping. The error associated with the calibration constant was found to be 22%, largely because the laminar flame was not truly steady, but exhibited fractionation due to the fixed pool of liquid. However, these errorbars were comparable with the overall uncertainty in the measurement of 21%, evaluated by a direct comparison of the LII derived extinction with a direct and independent measure of extinction. The LII measurement of extinction was found to be consistently lower than the actual extinction, consistent with the influence of signal trapping in the turbulent flame.

The time averaged soot volume fraction, $\bar{f}_v$ in the JP-8 pool fire was found to exhibit a peak value of about 0.40 ppm. This agrees quite well with the value measured elsewhere by a semi-intrusive measure for a larger flame [22], and is half an order of magnitude greater than the values measured in propane jet flames [20], consistent with a higher soot loading. This peak is located on the burner axis close to the burner surface at $x/d = 0.004$. The time averaged peak value is an order of magnitude lower than the peak instantaneous value, $f'_{v,\max}$, measured to be about 2.5 ppm. However, these values are probably slightly lower than the true values due to the combined effects of signal trapping and PAH attenuation. The radial distributions of $\bar{f}_v$ were found to decrease from the centerline to the edge in approximately a Gaussian fashion, and a comparison of soot volume fraction on the left and right side of the flame revealed a slight power loss in the LII signal intensity due to attenuation. The probability of not finding soot at a given location, termed the intermittency, I, was found to increase along the centerline of the pool fire from a low of about 35% near to the base, to be approximately constant at about 50% elsewhere. The total soot volume per meter, obtained by integrating $\bar{f}_v$ through planar disks, was measured to increase with height through the flame from 2.5 mm^2 to 3.5 mm^2, consistent with considerable soot being emitted from the flame. The probability density functions of f_v were found to be approximately exponential. However, the most probable value of f_v was slightly greater than zero where I was lowest, resulting in some departure from an exponential distribution for those conditions.

The simultaneous imaging of f_v by LII and of OH by planar LIF, performed in a JP-8 pool fire, revealed the generally expected trend of the OH typically being found in sheets adjacent to soot layers, confirming the reliability of the detection method. The sheets in a sample of the image pairs were visually sorted into four categories. Clear differences were found in the base and tip regions of the flame. On average, 52% of the OH sheets were found to exhibit a strong visual correlation to the shape of the soot sheets. However this correlation decreased from 80% at the base, to about 60% near to the tip. The probability that the OH was found predominantly on the outside (RHS) of the OH was found to decrease from approximately 60% near the base to less than 10% near to the tip, consistent with increased dynamics of the large structures with height, under the influence of buoyancy. Likewise, the number of events in which soot was judged to be "breaking through" the reaction zone marked by OH, and into the oxidizer stream, was found to increase from zero at the flame base to around 35% near to the tip. This implies an important role of large-scale dynamics in the escape of soot from the flame.

Acknowledgments

This work was sponsored by the Center for the Simulation of Accidental Fires and Explosions at the University of Utah, which was funded by the U.S. Department of Energy under Contract No. LLL B341493, with matching funds provided by the University of Utah Research Fund. The Fluid Mechanics, Energy and Combustion Group at the University of Adelaide, and the Australian Research Council provided experimental support. The authors would like to gratefully acknowledge the support of Dr. Keith King at the University of Adelaide; Dr. Adel Sarofim, and Mr. Dana Overacker at the University of Utah.

References

[1] R.S. Barlow, Sandia H2/He Flame Data – Release 2.0, Sandia National Laboratories, 2003. Available from: <http://www.ca.sandia.gov/TNF>.
[2] R.S. Barlow, C.D. Carter, Combust. Flame 97 (1994) 261–280.
[3] R.S. Barlow, C.D. Carter, Combust. Flame 104 (1996) 288–299.
[4] Y. Xin, J. Gore, in: 35th National Heat Transfer Conference, June 10–12, 2001.
[5] K. Koshe-Honehaus, J.B. Jeffries, Applied Combustion Diagnostics, Taylor and Francis, New York, 2002.
[6] K.P. Geigle, Y. Schneider-Kuhnle, M.S. Tsurikov, R. Hadef, R. Luckerath, V. Kruger, W. Stricker, M. Aigner, P.E. Bengtsson, G. Smallwood, Proc. Combust. Inst. 30 (2005) 1645–1653.
[7] M.S. Tsurikov, K.P. Geigle, V. Kruger, Y. Schneider-Kuhnle, W. Sticker, R. Luckrath, R. Hadef, M. Aigner, Combust. Sci. Technol. 177 (2005) 1835–1862.
[8] L.L. McCrain, W.L. Roberts, Combust. Flame 140 (2005) 60–69.
[9] K.A. Thomson, D.R. Snelling, G.J. Smallwood, F. Liu, Appl. Phys. B 83 (2006) 469–475.
[10] J. Reimann, S. Wil, Microgravity Sci. Technol. 16 (2005) 333–337.
[11] L.M. Pickett, J.B. Ghandi, Combust. Flame 132 (2003) 138–152.
[12] M. Commodo, S. Violi, A. D'Anna, A. D'Alessio, C. Allouis, F. Beretta, P. Minutolo, Combust. Sci. Technol. 179 (2007) 387–400.
[13] Y. Xin, J.P. Gore, Proc. NHTC 1 (2001) 923–929.
[14] C.R. Shaddix, J.E. Harrington, K.C. Smyth, Combust. Flame 99 (1994) 723–732.
[15] C.R. Shaddix, K.C. Smyth, Combust. Flame 107 (1996) 418–452.
[16] D.R. Snelling, G.J. Smallwood, R.A. Sawchuk, W.S. Neil, D. Gareau, D.J. Clavel, W.L. Chippior, F. Liu, O.L. Gulder, W.D. Bachalo, SAE Technical Paper Series, Warrendale, PA, 2000.
[17] A. Boiarciuc, F. Foucher, C. Mounaim-Rousselle, Appl. Phys. B 83 (2006) 413–421.
[18] A. Boiarciuc, F. Foucher, B. Moreau, O. Pajot, C. Mounaim-Rousselle, in: Proceedings of the 12th International Symposium on Application of Laser Techniques to Fluid Mechanics, Lisbon, 2004.
[19] D.R. Snelling, G.J. Smallwood, R.A. Sawchuk, W.S. Neil, D. Gareau, W.L. Chippior, F. Liu, O.L. Gulder, SAE Technical Paper 1999-01-3653, Warrendale, PA, 1999.
[20] N. Qamar, G.J. Nathan, Z.T. Alwahabi, K.D. King, Proc. Combust. Inst. 30 (2005) 1493–1500.
[21] T.R. Meyer, S. Roy, S.P. Gogineni, V.M. Belovich, E. Corporan, J.R. Gord, Proc. ASME Turbo Expo: Combust. Fuels Educ. 1 (2004) 827–836.
[22] J.J. Murphy, C.R. Shaddix, Combust. Sci. Technol. 178 (2006) 865–894.
[23] Y. Xin, J.P. Gore, G.J. Nathan, M.A. Mikofski, K.P. Geigle, Proc. Combust. Inst. 30 (2005) 719–726.
[24] N. Qamar, Z.T. Alwahabi, Q.N. Chan, G.J. Nathan, D. Roekaerts, in: Proceedings of the Australian Combustion Symposium, University of Sydney, December 9–11, 2007, pp. 42–45.
[25] R.W. Schefer, M. Namazian, J. Kelly, Opt. Lett. 16 (11) (1991) 858–861.
[26] S.H. Starner, R.W. Bilger, R.W. Dibble, R.S. Barlow, D.C. Fourguette, M.B. Long, Int. Symp. Combust. 24 (1992) 341–349.
[27] C.D. Carter, J.M. Donobar, J.F. Driscoll, Appl. Phys. B: Lasers Opt. 66 (1) (1998) 129–132.
[28] N. Qamar, Z.T. Alwahabi, Q.N. Chan, G.J. Nathan, D. Roekaerts, Combust. Flame, in press, doi:10.1016/j.combustflame.2009.02.011.
[29] D.A. Kliner, R.L. Farrow, J. Chem. Phys. 110 (1999) 412–422.
[30] E.G. Eddings, S. Yan, W. Ciro, A.F. Sarofim, Combust. Sci. Technol. 177 (2005) 715–735.
[31] T.L. Henriksen, Ph.D. Thesis, The University of Utah, May 2008.
[32] M.Y. Choi, K.A. Jensen, Combust. Flame 112 (1998) 485–491.
[33] J. Zhu, M.Y. Choi, G.W. Mulholland, S.L. Manzello, L.A. Gritzo, J. Suo-Anttila, Proc. Combust. Inst. 29 (2002) 2367–2374.
[34] T.L. Henriksen, G.J. Nathan, T.A. Ring, E.G. Eddings, Combust. Sci. Technol. 180 (4) (2008) 699–712.